SUBCORTICAL AMYLOID LOAD IS ASSOCIATED WITH SHAPE AND VOLUME IN COGNITIVELY NORMAL INDIVIDUALS

Running title: Subcortical Aβ associates to morphometry

Shady Rahayel,[a,b] Christian Bocti,[c] Pénélope Sévigny Dupont,[a,b] Maude Joannette,[a,b] Marie Maxime Lavallée,[a,b] Jim Nikelski,[d] Howard Chertkow,[d,e] Sven Joubert[a,b]

(a) Department of Psychology, Université de Montréal, Montreal, Canada
(b) Research Centre, Institut universitaire de gériatrie de Montréal, Montreal, Canada
(c) Department of Neurology, Université de Sherbrooke, Sherbrooke, Canada
(d) Lady Davis Institute for Medical Research, Jewish General Hospital, McGill University, Montreal, Canada
(e) Department of Neurology and Neurosurgery, McGill University, Montreal, Canada

Contact information of corresponding author:
Shady Rahayel
Research Centre, Institut universitaire de gériatrie de Montréal
4565, Chemin Queen-Mary
Montreal, Quebec, Canada
H3W 1W5
E-mail: shady.rahayel@gmail.com

ACKNOWLEDGEMENTS

This work was supported by a grant from the Canadian Institutes of Health Research (MOP123376) and the Institute of Aging (IA0120269). Christian Bocti declares investment in IMEKA. None of the other authors declares any conflicts of interest.

DATA AVAILABILITY STATEMENT

The data that support the findings of this study are available from the corresponding author upon reasonable request.

ABSTRACT (200 words)

Amyloid-beta (Aβ) deposition is one of the main hallmarks of Alzheimer's disease. The study assessed the associations between cortical and subcortical ^{11}C-Pittsburgh Compound B retention, namely in the hippocampus, amygdala, putamen, caudate, pallidum, and thalamus, and subcortical morphology in cognitively normal individuals. We recruited 104 cognitive normal individuals who underwent extensive neuropsychological assessment, PiB-positron emission tomography (PET) scan and 3-tesla magnetic resonance imaging (MRI) acquisition of T1-weighted images. Global, cortical, and subcortical regional PiB retention values were derived from each scan and subcortical morphology analyses were performed to investigate vertex-wise local surface and global volumes, including the hippocampal subfields volumes. We found that subcortical regional Aβ was associated with the surface of the hippocampus, thalamus, and pallidum, with changes being due to volume and shape. Hippocampal Aβ was marginally associated with volume of the whole hippocampus as well as with the CA1 subfield, subiculum, and molecular layer. Participants showing higher subcortical Aβ also showed worse cognitive performance and smaller hippocampal volumes. In contrast, global and cortical PiB uptake did not associate with any subcortical metrics. This study shows that subcortical Aβ is associated with subcortical surface morphology in cognitively normal individuals. This study highlights the importance of quantifying subcortical regional PiB retention values in these individuals.

KEYWORDS (up to 7)

Alzheimer's disease

Amyloid-beta

Subcortical

Volume

Shape

INTRODUCTION

Amyloid-beta (Aβ) deposition is one of the main hallmarks of Alzheimer's disease (AD) and may be present for decades when cognitive symptoms are clinically recognized (Braak & Braak, 1997; Villemagne et al., 2013). Aβ binding ligands such as ^{11}C-Pittsburgh compound B (PiB) allow for in vivo quantification of Aβ in the brain (Klunk et al., 2004; Murray et al., 2015). Several studies have investigated morphological changes in gray matter that are associated with Aβ load, primarily in patients with AD or mild cognitive impairment (MCI) (for a review, see de Flores, La Joie, & Chételat, 2015). However, in order to understand the prodromal mechanisms that may lead to AD, it is important to study these associations in individuals who do not yet present with cognitive impairment; only a few studies have investigated these associations in cognitively normal individuals.

Most studies in this line of research have focused on the volume of the hippocampus and its subfields across disease stages, with the most consistent findings being volume loss in the CA1 subfield and subiculum (de Flores et al., 2015). However, the association between baseline amyloidosis and longitudinal change in hippocampal volume in cognitively normal individuals remains unclear. Several studies have used other morphometric approaches to investigate the surface in the hippocampus (Csernansky et al., 2005; de Flores et al., 2015; Kalin et al., 2017; Tang et al., 2014), which revealed local modifications that did not necessarily translate into changes in the overall size of the structures (Patenaude, Smith, Kennedy, & Jenkinson, 2011). Such approaches have mainly revealed inward surface displacement in regions corresponding to the CA1 subfield and subiculum in AD and MCI patients (de Flores et al., 2015; Kalin et al., 2017) but also surface changes in the amygdala and the lateral ventricles (Tang et al., 2014). In cognitively normal individuals, surface deformation has also been found in association to Aβ burden in the hippocampal head and body and in the thalamus (Achterberg et al., 2014; Carmichael et al., 2012; Csernansky et al., 2005; Schroeder et al., 2016). In comparison to using overall volume values, surface changes were also shown to improve the detection of future cognitive changes (Csernansky et al., 2005; Carmichael et al., 2012; Achterberg et al., 2014).

Studies that investigated the effect of Aβ on subcortical morphology in cognitively healthy individuals differed considerably in their measures of PiB retention values (Villeneuve et al., 2015). Despite some evidence showing that cortical Aβ associates with cognitive decline and hippocampal atrophy in cognitively normal individuals (Andrews et al., 2013; Villemagne et al., 2011), several authors have used approaches based on regional PiB retention by using regions that are more vulnerable to Aβ (Seo et al., 2017; Villeneuve et al., 2015). In this line of thought, regional PiB retention in subcortical structures appears as a promising candidate for improving the prediction of cognitive impairment and cognitive decline (Cho et al., 2018). Moreover, a recent PET staging of amyloidosis showed that high Aβ in the striatum predicted hippocampal atrophy and cognitive impairment better than cortical Aβ (Hanseeuw et al., 2018a). In addition, in contrast to cortical PiB retention, only retention in the hippocampus revealed inward and outward surface changes in the CA1 subfield and subiculum regions in cognitively normal individuals (Schroeder et al., 2016). However, the effect of subcortical regional Aβ on subcortical morphology in cognitively normal individuals remains to be understood.

In this study, we investigated the effect of PiB retention in the cortex and in several subcortical structures, namely the hippocampus, amygdala, basal ganglia, and thalamus on the overall volume and the local surface of subcortical structures (including the hippocampal subfields) in cognitively normal individuals. We also investigated whether Aβ-associated surface changes were primarily due to changes in local volume or shape. We then elaborated a staging model of cerebral Aβ based on cortical and subcortical PiB uptake in order to understand the demographic, cognitive, and morphological characteristics of participants showing higher subcortical Aβ load. We hypothesized that the regional Aβ quantification would reveal more associations with subcortical surface morphology, especially in the hippocampus, than when using cortical PiB retention or global volumes of structures. We also hypothesized that participants with higher subcortical Aβ deposition would show lower performance in episodic memory and smaller hippocampal volumes.

MATERIALS AND METHODS

Subjects

A total of 104 participants aged 65 years and older were recruited through the participant pool of the Centre de recherche de l'Institut universitaire de gériatrie de Montréal (CRIUGM) (~900 participants) as well as via advertisements and word of mouth. The study protocol included extensive neuropsychological assessment, PiB-PET scan, and MRI data acquisition for every participant. To ensure that all participants included in our study were cognitively normal (i.e., free of dementia and MCI), the Montreal Cognitive Assessment (MoCA) was used as a screening tool and participants scoring below 23 were excluded; this score is considered the optimal screening threshold for a diagnosis of MCI using the MoCA (Carson, Leach, & Murphy, 2018). Exclusion criteria included untreated diabetes, vascular disease or another health condition that may have had deleterious effects on cognition (including mental health disorders), a history of moderate to severe traumatic brain injury or other neurological disorder as well as general anesthesia in the last six months. Participants also had to perform within ±1.5 SD from the mean of age-matched controls on at least one of two learning tasks: the Logical Memory subtest from the Wechsler Memory Scale—Third Edition (WMS-III) and the two-minute delay from the DMS-48. Participants also had to score less than 11 on the Geriatric Depression Scale (GDS). Then, a detailed neuropsychological assessment (see below) was performed in every participant to ensure that they were free of dementia and MCI; they also did not express any significant subjective memory complaints at the time of their participation. Research protocols were reviewed and approved by local research ethics boards. All subjects gave their informed consent prior to their participation in the study.

Cognitive assessment

Every participant underwent an extensive neuropsychological assessment from which seven composite scores were calculated: episodic memory (delayed free recall from the WMS-III; delayed free recall from the RAVLT), working memory (Digit Span and Arithmetic subtests from the WAIS-IV), executive functions (number-letter switching condition of the Trail Making Test—D-KEFS; sum of perseverative responses from the WCST), language (Vocabulary and Information subtests from the WAIS-IV; 30-item

BNT; letter and category fluency test), attention (number of omissions from the CPT-II; concentration performance from the d2 Test of Attention), processing speed (Symbol Search and Coding subtests from the WAIS-IV; motor speed condition of the Trail Making Test—D-KEFS), and visuospatial abilities (Block Design and Matrix Reasoning subtests from the WAIS-IV; Benton Judgment of Line Orientation Test). Raw scores were converted into standardized z scores based on the mean and standard deviation of all participants and averaged together to produce a composite z score for each cognitive domain.

PET acquisition and processing

PET imaging was conducted at the McConnell Brain Imaging Centre at McGill University on a Siemens/CTI ECAT HR+ scanner in 3D imaging mode (63 parallel planes). The PET scanning session allowed for the acquisition of 7 dynamic frames made up of 63 axial slices using a 128x128 matrix (voxel dimensions: x=2.059 mm, y=2.059 mm, z=2.425 mm). The participants underwent a 40-minute PET scan (7 frames: 6x300 seconds and 1x600 seconds) 50 minutes after an intravenous bolus injection of ^{11}C-PiB.

The post-acquisition processing proceeded in two dependent stages: (1) submission of all structural volumes (see next section) to the CIVET pipeline, and (2) subsequent processing of PET volumes via the Beagle pipeline. The CIVET pipeline (version 1.1.11), developed at the Montreal Neurological Institute (MNI) for the fully automated analysis of structural images (Ad-Dab'bagh et al., 2006), produced a wide range of products, including gray and white matter masks and transformations from native into standardized space (ICBM152). These products were subsequently injected into the Beagle multi-modal analysis pipeline (Nikelski, Chertkow, & Evans, 2012), which performed a wide range of tasks, including alignment of the dynamic volume to the structural, image transformation and resampling into ICBM152 space, and spatial smoothing to increase signal-to-noise using a 6-mm full-width at half-maximum kernel. Once dynamic volume preprocessing was complete, the Beagle pipeline quantified PiB load at each voxel by dividing the PiB signal at the voxel by the average signal strength measured within the cerebellar gray matter (the reference tissue). Cerebellar grey matter was used as the reference because it is largely spared from

Aβ deposition (Klunk et al., 2004). As such, ratio values >1.0 identified those voxels exhibiting a PiB-related signal of greater magnitude than that found within the cerebellum. In order to confirm the robustness of our findings, we performed similar analyses with uptake values derived from using subcortical white matter as the reference region. No partial volume correction was performed in this study due to having included participants who were considered cognitively healthy after a thorough neuropsychological assessment and who were therefore not expected to show significant atrophy on brain MRI scans.

Ratio values were then used to produce both global and localized (region of interest (ROI)-based) metrics. Several standardized uptake value ratio (SUVr) values were computed by creating an average comprised of the values at either all gray matter voxels (global PiB retention value), only those from the cortical surface (cortical PiB retention value), or only those from a set of subcortical structures (subcortical regional PiB retention values). On average, the global PiB retention value was made up of 93% (n=613,993) cortical voxels and 7% (n=45,961) subcortical voxels (hippocampus, amygdala, caudate, putamen, pallidum, and thalamus). The ROI-based values were produced by non-linearly fitting a modified version of the Automated Anatomical Labeling template (Tzourio-Mazoyer et al., 2002) to the ratio values volume, thus permitting us to compute average ratio values for the 120 ROIs included in the template. The cortical PiB retention values were the average of the values at all gray matter voxels comprising the cortical surface. Twelve subcortical regional PiB retention values were also derived, namely from the left and right hippocampus, amygdala, putamen, caudate nucleus, pallidum, and thalamus. Global, cortical, and regional subcortical PiB retention values were used as continuous variables for regression analyses with the other structurally-based subcortical metrics.

MRI acquisition and processing

MRI acquisition

All imaging data were acquired using a 3T Siemens TrioTIM MR scanner (Siemens, Erlangen, Germany) at the Unité de neuroimagerie fonctionnelle of the Institut universitaire de gériatrie de Montréal. High-resolution T1-weighted images were acquired using a magnetization-prepared rapid acquisition with gradient-echo (MPRAGE)

sequence, with the following parameters: TR=2.3 s, TE=2.94 ms, TI=900 ms, flip angle=9 degrees, FOV=256x240, voxel size: 1mm x 1mm x 1.2 mm. PiB-PET imaging and MRI scan acquisition both took place within a year, within an average of 89 days.

Processing of the overall volumes of subcortical structures

Processing of the overall volumes of subcortical structures was aimed at generating one volume measurement for every subcortical structure of interest. As a first step, segmentation of subcortical volumes was performed semi-automatically from each individual's T1-weighted image using the FreeSurfer segmentation pipeline, version 6.0, which has been described in detail elsewhere (Fischl et al., 2002; Fischl et al., 2004). This approach performs registration to standard space, intensity inhomogeneity correction, removal of non-brain tissue, tissue-type classification, and probabilistic anatomical labeling. Quality control was conducted at each step and processing that yielded bad results were excluded. This approach generated raw volume measurements for the following deep gray matter nuclei: the left and right amygdala, putamen, caudate nucleus, pallidum, and thalamus. The overall volumes derived from these subcortical nuclei are referred to as 'subcortical overall volumes' in this manuscript.

As a second step, we also performed semi-automatic segmentation of hippocampal subfields using the hippocampal subfield module available as part of FreeSurfer, version 6.0 (Iglesias et al., 2015). This approach is based on Bayesian inference using an atlas algorithm of the hippocampal formations built upon ultra-high resolution (~0.1 mm isotropic) ex vivo MRI data from autopsy brains (Iglesias et al., 2015). It allows for the segmentation of the whole hippocampus (as one of the subcortical overall volumes) and of 24 hippocampal subfields, namely the left and right CA1, CA2/3, CA4, dentate gyrus, hippocampal-amygdalar transition area, fimbria, alveus, molecular layer, parasubiculum, presubiculum, subiculum, hippocampal fissure, and hippocampal tail. This approach was shown to delineate with greater accuracy the boundaries within subfields, thus outperforming previously released FreeSurfer segmentation modules (e.g., version 5.3), which did not translate well to some hippocampal subfields (de Flores et al., 2015; Iglesias

et al., 2015). Volumes derived from this approach are referred to as 'hippocampal subfields volumes' in this manuscript.

Processing of subcortical local surface

Processing of the local surface of subcortical structures was aimed at generating a surface mesh for every subcortical structure mentioned previously in order to perform vertex-wise (local) analysis of surface displacement. Surface processing was therefore performed for the left and right hippocampus, amygdala, putamen, caudate nucleus, pallidum, and thalamus using FIRST, version 5.0.11 (Patenaude et al., 2011), part of FSL (Jenkinson, Beckmann, Behrens, Woolrich, & Smith, 2012). Subcortical segmentation was first performed semi-automatically from each subject's T1-weighted image. Each structure was modeled as a surface mesh based on shape and intensity information from a dataset of 336 manually delineated T1-weighted images (Patenaude et al., 2011). A ventricle-specific weighting mask was also applied in all participants to optimize registration to the standard space. Since surfaces resided in native space, vertices were registered into the MNI152 space in order to compare surface between subjects. This allowed for analyzing surface displacement due to local volume or shape and surface displacement due to shape only (Patenaude et al., 2011; Tanner, McFarland, & Price, 2017). The first approach removed between-subjects changes due to pose (i.e., rotation and translation) by minimizing the sum of squared errors between the corresponding vertices of a participant's surface and the mean target surface; surface information revealed by this approach relates to the effect of both local volume and shape. In contrast, the second approach used a similar processing but with adjustment of the models for scaling; surface information revealed by this approach detects differences in shape even if the overall volume remains similar (i.e., surface changes that were still significant after having removing the effect of size and global scalings when aligning meshes).

Statistical analysis

Subcortical global volume analysis

Statistical analyses were performed using IBM SPSS Statistics, version 22.0 (IBM Corp., Armonk, NY). All raw overall volume measurements were normalized for brain size before

conducting any statistical analyses. Subcortical global volumes were normalized by dividing the raw volume by the subject's estimated total intracranial volume (TIV), calculated as part of the FreeSurfer segmentation pipeline. Hippocampal subfields volumes were also normalized following this procedure. Therefore, all statistical analyses on subcortical global volumes were normalized for head size.

To investigate the associations of subcortical overall volumes and hippocampal subfields volumes with global and cortical regional PiB retention values, partial correlations were performed with age and sex as covariates. Age and sex were used as covariates since they correlated with PiB retention values and subcortical overall volumes and hippocampal subfields volumes. In contrast, education was not used as a covariate since it did not associate significantly with any PiB retention values or subcortical volumes. For correlations with subcortical regional PiB retention, global PiB retention was also added as a covariate in order to investigate the impact of subcortical Aβ load specifically. For each set of partial correlations, associations with global, cortical, and regional PiB retention values were considered statistically significant at $p<0.05$ when corrected for multiple comparisons using a Bonferroni-corrected threshold. Regarding subcortical regional PiB retention values, only corrections between a structure's normalized volume and the PiB retention value derived from this structure were conducted. Similarly, associations between hippocampal subfields volumes and subcortical regional PiB values were only performed in the left and right hippocampus. Despite significance being considered at $p<0.05$ corrected for multiple comparisons, we also interpreted results as statistical trends when $p<0.05$ without correction for multiple comparisons.

Subcortical surface analysis

To investigate the associations between subcortical surface and global, cortical, and regional Aβ loads, we first performed vertex-wise 'shape considering volume' (i.e., surface changes due to volume and/or shape) and then 'shape only' (i.e., surface changes due to shape only) analyses to better understand whether the likeliest structural contributor to significant associations with surface. Associations with global and cortical PiB retention values were conducted with local surface in all subcortical structures; associations with

regional PiB retention values were performed only with the local surface of the structure from which the PiB value was derived (e.g., associations between PiB value in the left hippocampus and the local surface of the left hippocampus). Moreover, associations with hippocampal subfields volumes were only performed with global, cortical, and regional PiB retention values in the left and right hippocampus only.

Local surface displacement represented the vertex projections between each individual's surface and the mean surface mesh, which were stored as scalar values. In order to use the most appropriate statistical model for each analysis, we explored the effects of age, sex, and education on local subcortical surface in every subcortical structure by conducting shape considering volume and shape only analyses, with local surface displacement values as regressands and the covariate as regressor (separately). Age was significantly associated with subcortical surface and sex differences were found in the hippocampus, caudate, putamen, and thalamus. Years of education did not correlate significantly with subcortical surface either when performing analyses with and without taking into account global scalings. Therefore, in all regression models, local surface displacement values were used as regressands, PiB retention values as regressors, and age (and sex when appropriate) as covariates. All analyses involving subcortical PiB retention values also included global PiB uptake as a covariate in order to investigate specifically the effect of subcortical Aβ load on subcortical surface. TIV was not included as a covariate in the models since surface meshes were reconstructed in the MNI152 space, controlling for head size (Patenaude et al., 2011). Vertex-wise statistical analyses were performed using FSL's *randomise* tool for nonparametric permutation inference (Winkler, Ridgway, Webster, Smith, & Nichols, 2014), using 10,000 permutations (Nichols & Holmes, 2002) together with a threshold-free cluster enhancement (TFCE) approach (Smith & Nichols, 2009). Resulting statistical maps were thresholded at $p<0.05$ corrected for multiple comparisons; clusters surviving this threshold were considered significant. Only clusters that were at least 30 vertices in size were considered significant in order to avoid interpretation of marginal results.

Staging of brain amyloidosis

Similarly to previous studies (Hanseeuw et al., 2018a; Cho et al., 2018), every participant was classified according to a staging of cerebral Aβ based on the PiB retention values derived from the cortex and the subcortical regions in which Aβ-associated surface effects were identified. First, we identified cut-off scores in order to classify every participant as Aβ-positive or Aβ-negative in terms of their cortical PiB uptake. Based on a previous study (Villeneuve et al., 2015), we used a Gaussian mixture model and the Bayesian information criterion to investigate the distributions underlying the participants' cortical PiB retention values and to find the optimal number of distributions that fit our data. Two distributions were found to estimate best the distribution of cortical PiB uptake, which were considered to reflect participants who were Aβ-positive (i.e., elevated Aβ retention in the cortex) and participants who were Aβ-negative (i.e., normal Aβ retention in the cortex). A cut-off was derived that represented the 90% probability of belonging to the Aβ-negative distribution; every participant whose cortical PiB retention value ≥1.22 was therefore considered Aβ-positive based on the cortex. This cut-off is very similar to the one reported previously using a similar method (1.21; Villeneuve et al., 2015).

Second, we classified the participants as Aβ-positive or Aβ-negative based on subcortical PiB uptake; only participants who had high Aβ retention in the cortex were classified as Aβ-positive or Aβ-negative on subcortical PiB retention based on previous studies showing that subcortical Aβ accumulation is likely to happen once the cortex shows Aβ deposition (Thal et al., 2002; Beach et al., 2012). To determine Aβ positivity on subcortical structures, we derived a subcortical PiB index for each participant based on the mean of PiB retention values from the structures in which surface was shown to be influenced by the presence of Aβ, namely the left and right hippocampus, the left and right thalamus, and the right pallidum (see Results). Since only a portion of these structures showed Aβ-associated effects, the subcortical PiB index was weighted according to the number of vertices comprised in the cluster in which volume/shape was associated with regional Aβ (see Table 3 for the number of vertices in each cluster). Based on a previous study (Cho et al., 2018), the resulting subcortical PiB index (one per participant) was then standardized based on the whole cohort of 103 participants and subcortical Aβ positivity was determined when

an already Aβ-positive participant on the cortex showed a z score of subcortical PiB uptake ≥1.00. Participants with low cortical and subcortical Aβ retention were considered at Stage 0, participants with increased cortical retention but low subcortical Aβ retention at Stage 1, and participants with increased cortical and subcortical retention levels at Stage 2.

In order to investigate the clinical and brain characteristics of the different Aβ stages, we then conducted a series of exploratory analyses of variance between the three groups on the demographic and cognitive variables and on the subcortical overall volumes and hippocampal subfields volumes. Tukey's post-hoc tests were used to investigate pairwise differences. We interpreted differences when at $p<0.05$ uncorrected for multiple comparisons.

RESULTS

Participants

A total sample of 104 cognitively normal individuals (mean age: 73.4 years; 75% women; mean education level: 13.7 years; mean MoCA score: 27.3) were recruited, but 1 was removed due to registration failure during imaging processing (total sample = 103 participants). Demographics, clinical variables, and PiB retention values for the total sample are available in Table 1.

Subcortical global volume analyses

A summary of the values of subcortical overall volumes and hippocampal subfields volumes for the whole sample is available in Table 2. Investigation of the associations of the global and cortical PiB retention values with normalized volumes of subcortical structures, namely the left and right hippocampus, amygdala, putamen, caudate nucleus, pallidum, and thalamus, revealed no significant relationships ($p>0.2$) (see Supporting Information for results). In contrast, subcortical regional PiB retention values correlated positively with volume of the left hippocampus (i.e., positive association between Aβ load in the left hippocampus and volume of the left hippocampus, $r=0.205$, $p=0.040$) and negatively with volume of the right putamen ($r=-0.214$, $p=0.032$) (Fig. 1A). However, these correlations did not remain significant after correction for multiple comparisons ($p<0.004$).

Investigation of the associations between global and cortical PiB retention values and hippocampal subfields volumes revealed no significant relationships ($p>0.2$) (see Supporting Information for results). However, when investigating associations between PiB retention values in the left and right hippocampus (separately) and hippocampal subfields volumes, PiB retention in the left hippocampus correlated positively with volumes of the left CA1 ($r=0.218$, $p=0.029$), subiculum ($r=0.248$, $p=0.013$), and molecular layer ($r=0.241$, $p=0.016$) (Fig. 1B and 1C). However, none of these correlations remained significant after correction for multiple comparisons ($p<0.004$).

When using subcortical white matter as the reference for quantifying ratio values, results were similar, with global and cortical Aβ not being associated with volumes and with Aβ in the left hippocampus being related to increased volume of the whole structure as well as with increase for the CA1 subfield, subiculum, and molecular layer. However, increased Aβ in the left hippocampus was now also related to volume of the CA4 subfield, the granule cell and molecular layers of the dentate gyrus and the hippocampal tail (see Supporting Information). Aβ in the left thalamus was now associated with its volume but the previous correlation between Aβ in the right putamen and its overall volume now became borderline ($r=0.051$).

Subcortical surface analyses

When investigating Aβ-related surface changes that are due to local volume or shape (i.e., without removing the effect of size from the analyses), we did not find any significant associations between global and cortical PiB retention values and local surface in any of the subcortical structures. Instead, when using subcortical regional PiB retention values, significant associations with outward surface displacement were found in the bilateral hippocampus and thalamus and in the right pallidum (Table 3 and Fig. 2). Specifically, PiB retention in the left hippocampus was associated with extensive surface expansion in regions corresponding to CA1 and the subiculum ($r=0.442$, $p<0.001$) (Fig. 2A). Similar associations, although less extensive in size, were found between PiB retention in the right hippocampus and surface expansion in the subiculum and CA1 (anterior cluster: $r=0.299$,

p=0.002; posterior cluster: r=0.376, p<0.001) (Fig. 2B). PiB retention in the left and right thalamus both correlated significantly with extensive surface expansion on the medial and lateral surfaces of the left (r=0.351, p<0.001) and right thalamus (r=0.331, p=0.001) (Fig. 2C and 2D). In addition, PiB retention in the right pallidum was associated with surface expansion on the ventromedial (r=0.331, p=0.001) and the dorsomedial and lateral surface (r=0.255, p=0.010) of the right pallidum (Fig. 2E). There were no associations between regional PiB retention and inward surface displacement in subcortical structures. When using subcortical white matter as the reference, results remained similar for the bilateral thalamus, similar but less extensive for the right hippocampus, and were no longer significant for the left hippocampus and the right pallidum (see Supporting Information). Global and cortical PiB uptake still did not reveal significant associations with subcortical surface morphology.

When investigating Aβ-related surface changes that are only due to local shape (i.e., by removing the effect of size from the analyses), surface analyses did not reveal any significant associations between global and cortical PiB retention values and local surface in any of the subcortical structures. However, when investigating associations with subcortical regional PiB retention values, significant associations were found with local surface in the bilateral thalamus and the right pallidum (Table 3 and Fig. 3). Specifically, PiB retention in the left and right thalamus correlated with shape contraction on the medial surface (left: r=-0.321, p=0.001; right: r=-0.389, p<0.001) and with shape expansion on the dorsal surface (left: r=0.310, p=0.002; right: r=0.299, p=0.002) of their respective structure (Fig. 3A and 3B). Qualitatively speaking, the clusters showing surface expansion overlapped with the clusters that were associated with thalamic Aβ load when using shape considering volume analyses. This is in contrast with the clusters showing surface contraction, which were found in regions of the thalamic surface that did not correlate with thalamic Aβ load when using shape considering volume analyses. PiB retention in the right pallidum was also associated with a small cluster of surface expansion on the ventromedial surface of the right pallidum (r=0.359, p<0.001) (Fig. 3C). This cluster qualitatively overlapped with the results found when using shape considering volume analyses. No other associations between subcortical regional PiB retention and shape were found in the

remaining subcortical structures, including the bilateral hippocampus. When using subcortical white matter as the reference, results remained similar but were less extensive, with PiB uptake in the left thalamus being associated with outward displacement and with inward displacement in the right thalamus (see Supporting Information). In addition, whereas higher PiB uptake in the right caudate was now associated with inward displacement of the surface, the association that we had in the right pallidum was no longer significant. Global and cortical PiB uptake were still unrelated to subcortical surface morphology.

Staging of amyloidosis

Every participant was classified into either one of three stages based on our model of Aβ staging of the PiB retention in the cortex and in subcortical regions in which an Aβ-associated effect on surface was found. Seventy-one (69%) participants were considered at Stage 0 (i.e., low cortical and subcortical PiB uptake), 26 (25%) participants at Stage 1 (i.e., high cortical but low subcortical PiB uptake), and 6 (6%) participants at Stage 2 (i.e., high cortical and subcortical PiB uptake). Compared to participants at Stage 1, participants at Stage 2 were older and had increased global and cortical PiB uptake, worse episodic memory performance, and smaller hippocampal subfields volumes, namely for the subiculum, presubiculum, and fimbria (Table 4). Participants at Stage 2 also had worse performance on tasks assessing attention and smaller overall volume for the right hippocampus compared to participants at Stage 0.

DISCUSSION

In this study, we investigated the subcortical changes in overall volume and local surface associated with global, cortical, and subcortical regional PiB retention values in cognitively normal individuals. We found that subcortical regional Aβ load was associated with surface displacement in the hippocampus, thalamus, and pallidum, as well as with trends for the overall volume of the hippocampus, particularly the CA1 subfield, subiculum, and molecular layer. In contrast, global or cortical PiB retention values did not associate with volume or surface in the hippocampus, amygdala, basal ganglia, and thalamus.

It has been proposed that Aβ pathology propagates hierarchically from the neocortex to the allocortical, diencephalic, and basal ganglia structures, reaching the brainstem and cerebellum in the more advanced pathological stages (Thal, Rub, Orantes, & Braak, 2002). Most studies that investigated morphological changes associated with Aβ have focused mainly on cortical PiB retention measured globally or within a set of predefined regions (Jack et al., 2017; Villeneuve et al., 2015). In this study, we showed that in cognitively normal individuals, subcortical Aβ was associated with morphological changes in the hippocampus, thalamus, and pallidum, which were not found when using global or cortical PiB retention values. This concurs with a recent study in AD, MCI, and cognitively normal individuals that demonstrated the limitations of cortical cut-offs; using various cut-offs based on cortical ligand retention, a high number of individuals were classified as Aβ-negative despite having abnormally elevated Aβ in at least 50% of wide parts of the frontal, temporal, and parietal association cortices, lower levels of CSF Aβ42, and lower episodic memory performance (Grothe et al., 2017). Also, in contrast with global cortical Aβ values, subcortical Aβ predicted cognitive decline with better accuracy than cortical Aβ (Hanseeuw et al., 2018a), suggesting that the use of global or cortical PiB retention values in cognitively normal individuals may overshadow some structural changes associated with accumulation of Aβ in subcortical structures. Therefore, our findings underline the importance of investigating the impact of Aβ accumulation in subcortical structures, especially since subcortical Aβ was shown to be associated with worse clinical outcomes (Beach et al., 2012; Cho et al., 2018; Hanseeuw et al., 2018a, b), including steeper cognitive decline and functional and structural abnormalities such as hippocampal atrophy (Cho et al., 2018). It is important to precise that our findings do not propose that Aβ accumulates preferentially in subcortical structures compared to the cortex but that its accumulation in subcortical structures allows revealing morphological changes in individuals still free of cognitive impairment. Indeed, it is thought that Aβ reaches global levels before cognitive impairments become clinically significant (Jack et al., 2010). The staging model of cerebral amyloidosis elaborated for the purpose of the present study supports that Aβ-associated surface changes have clinical significance in cognitively healthy individuals, namely that elderly subjects with high subcortical Aβ are older, show increased global and cortical PiB uptake, lower episodic memory and attention performance, and smaller hippocampal

volumes. However, in relation to future cognitive decline, cognitive follow-up of these individuals is currently under way and will inform on the importance of subcortical Aβ. Longitudinal data will also help addressing questions about whether subcortical cut-off values may prove useful in the identification of individuals more likely to develop MCI or AD (Edmonds et al., 2016).

In this study, Aβ load in the left hippocampus was marginally associated with the overall volume of the hippocampus, particularly with the CA1 subfield, subiculum, and molecular layer, which are the subregions preferentially affected in AD and MCI patients according to previous neuroimaging and histological studies (de Flores et al., 2015). In cognitively normal individuals, global Aβ burden has also been associated with smaller subiculum but findings also show abnormalities in the hippocampal tail (Hsu et al., 2015). Despite being in line with previous studies, none of our overall volume associations survived correction for multiple comparisons. A vertex-based surface approach was used to investigate Aβ-associated local surface changes in subcortical structures and whether these changes related more to local volume or shape. Surface-based approaches have proven efficient in the detection of subtle surface abnormalities in subcortical structures in AD, MCI, and cognitively normal individuals (Csernansky et al., 2005; de Flores et al., 2015; Kalin et al., 2017; Leh et al., 2016; Schroeder et al., 2016). Unlike our previous analyses using subcortical overall volumes, we found that subcortical regional PiB retention values were associated with the surface of the bilateral hippocampus and thalamus and the right pallidum. Surface displacement associated with hippocampal Aβ owed exclusively to local volume changes; these changes were located bilaterally in regions roughly corresponding to the CA1 subfield and subiculum and were more prominent in the left hippocampus, which is in line with previous shape-based investigations in AD and MCI patients reporting abnormal surface in the hippocampus (Csernansky et al., 2000; Leh et al., 2016; Lindberg et al., 2012). Lateral deformation of the hippocampus, which we also found in our study, was reported to predict cognitive decline and dementia onset in cognitively normal individuals (Csernansky et al., 2005; Zanchi, Giannakopoulos, Borgwardt, Rodriguez, & Haller, 2017). Similarly, cognitively normal individuals who later converted to MCI or AD showed abnormal surface at baseline in CA1 and subiculum (Apostolova et al., 2010;

Csernansky et al., 2005). In AD patients, surface changes in CA1 and subiculum were also related to lower neuronal counts (Blanken et al., 2017), suggesting that our findings in cognitively normal individuals may also relate to ongoing physiological processes in the hippocampus.

Extensive Aβ-associated surface change was also found in the bilateral thalamus, which was mostly due to changes in local volume and which followed a relatively symmetrical pattern. This concurs with the occurrence of significant amounts of Aβ in the thalamus of AD (Braak & Braak, 1991). Shape abnormalities in the thalamus associated with Aβ have also been reported in cognitively normal individuals (Schroeder et al., 2016) as well as in MCI patients who showed cognitive worsening over a two-year period (Kalin et al., 2017). Interestingly, we also found that some of the surface change in the thalamus were also due to changes in shape only (i.e., surface remains abnormal even when analyses were corrected for size and global scalings), particularly in regions which did not show surface changes when investigating the effect of local volume change. This suggests that even the investigation of local volume may not reveal the extent of the changes occurring in the thalamic surface. These changes due to shape only were symmetrical and found in regions corresponding to the medial thalamic nuclei, a region highly connected with the frontal lobes that plays a gating role in the hippocampal-prefrontal pathway activity and is involved in executive control, strategic retrieval of information in memory, and decision-making (Mitchell, 2015). It has been proposed that the onset of deficits in executive functions may in part result from the interference with prefrontal cortex functions caused by the pathology within the medial thalamic region (Aggleton, Pralus, Nelson, & Hornberger, 2016). The interplay between volume and shape on subcortical surface remains to be understood; it is possible that shape changes precede volume changes in subcortical structures, and that shape changes would eventually lead to local volume changes as those seen for the rest of the thalamus. As for the right pallidum, the surface was also associated with subcortical regional Aβ, primarily with its volume but also with a smaller cluster of shape. This concurs with shape changes having been reported in the pallidum in MCI patients (Tang et al., 2014; Yi et al., 2016). Of note, Aβ-associated surface changes in the right hippocampus and in the left and right thalamus were also found when

changing the reference region for quantifying SUVr values, suggesting that the effect of subcortical Aβ on these structures is robust.

We generally observed positive relationships between regional subcortical Aβ and morphology, associating with global volume increases and outward surface displacement. This contrasts with several studies reporting Aβ-related atrophy (de Flores et al., 2015) but concurs with other studies in cognitively normal individuals that reported increased volume and outward deformation in the thalamus and hippocampus in association with cortical and regional PiB retention (Chetelat et al., 2010; Schroeder et al., 2016). The exact role of Aβ dyshomeostasis in AD pathogenesis remains to be understood (Chételat, 2013), especially in light of other candidates such as tau tangles and other novel proteomics targets associated with cognitive decline but independent from Aβ (Xia et al., 2017; Yu et al., 2018). In addition, a very high level of heterogeneity in neuropathologic comorbidity has been observed at a person-specific level, with more than 200 distinct combinations of neuropathologies being reported and with 78% of participants showing mixed neuropathology (Boyle et al., 2018). Therefore, the subcortical surface changes found in our study can only be said to be associated with Aβ and cannot yet be linked to other neurodegenerative candidates. Our findings of hypertrophy are however congruent with previous evidence of neuroinflammation in AD (Heneka et al., 2015). Increased microglial activation has been reported in MCI and early AD patients (Fan, Brooks, Okello, & Edison, 2017; Hamelin et al., 2016; Parbo et al., 2017) and has been linked to better cognitive performance and increased gray matter volume (Hamelin et al., 2016). Increased microglial activation has also been associated with Aβ deposition more than tau tangles in AD and MCI patients (Parbo et al., 2017; Parbo et al., 2018). In AD, hippocampal shape expansion was associated with anti-inflammatory parameters and surface contraction with pro-inflammatory parameters (Cabinio et al., 2018). The increased hippocampal volumes and the outward surface displacements that we found in subcortical structures may be early morphological changes in cognitively normal individuals that hypothetically appear in response to Aβ-related neuroinflammatory processes. However, this hypothesis is highly speculative and whether neuroinflammation has an explanatory role in our associations remains a matter of investigation.

This study had some limitations. First, in this study, we only reported baseline results from our cohort of cognitively normal individuals. Our cohort is followed longitudinally to assess the development of cognitive impairment, which will allow a clearer understanding of the associations between volume and shape changes and cognitive decline. Second, we did not account for the presence of apolipoprotein-E ε4, a well-known risk factor for sporadic AD. Some of our effects may therefore have been influenced by the presence of some ε4-carriers. However, our cognitive assessment was thorough and all participants were carefully screened for cognitive impairment. Third, we did not apply any partial volume correction in the quantification of SUVr values. However, our elderly participants all had normal cognitive functions as confirmed by a thorough neuropsychological assessment and our pattern of results remained relatively similar when changing the reference region for quantifying SUVr values, particularly the right hippocampus and the left and right thalamus.

CONCLUSION

In summary, regional Aβ in the hippocampus, thalamus, and pallidum is associated in cognitively normal individuals with surface in these structures. These associations were not found when using global or cortical PiB retention values or when using global subcortical volumes. Elderly participants with normal cognition but who show higher levels of subcortical PiB uptake were older and had worse episodic memory and attention performance, increased global and cortical PiB uptake, and smaller hippocampal volumes. This highlights the importance, in cognitively normal individuals, of investigating the regional PiB retention in subcortical structures to better understand the neuropathological signature of AD.

REFERENCES

Achterberg, H. C., van der Lijn, F., den Heijer, T., Vernooij, M. W., Ikram, M. A., Niessen, W. J., & de Bruijne, M. (2014). Hippocampal shape is predictive for the development of dementia in a normal, elderly population. *Hum Brain Mapp, 35*(5), 2359-2371. doi:10.1002/hbm.22333

Ad-Dab'bagh, Y., Lyttelton, O., Muehlboeck, J. S., Lepage, C., Einarson, D., Mok, K., . . . Evans, A. C. (2006). *The CIVET image-processing environment: A fully automated comprehensive pipeline for anatomical neuroimaging research.* Paper presented at the Proceedings of the 12th Annual Meeting of the Organization for Human Brain Mapping.

Aggleton, J. P., Pralus, A., Nelson, A. J., & Hornberger, M. (2016). Thalamic pathology and memory loss in early Alzheimer's disease: moving the focus from the medial temporal lobe to Papez circuit. *Brain, 139*(Pt 7), 1877-1890. doi:10.1093/brain/aww083

Andrews, K. A., Modat, M., Macdonald, K. E., Yeatman, T., Cardoso, M. J., Leung, K. K., . . . Australian Imaging Biomarkers, L. F. S. o. A. (2013). Atrophy rates in asymptomatic amyloidosis: implications for Alzheimer prevention trials. *PLoS One, 8*(3), e58816. doi:10.1371/journal.pone.0058816

Apostolova, L. G., Mosconi, L., Thompson, P. M., Green, A. E., Hwang, K. S., Ramirez, A., . . . de Leon, M. J. (2010). Subregional hippocampal atrophy predicts Alzheimer's dementia in the cognitively normal. *Neurobiol Aging, 31*(7), 1077-1088. doi:10.1016/j.neurobiolaging.2008.08.008

Beach, T. G., Sue, L. I., Walker, D. G., Sabbagh, M. N., Serrano, G., Dugger, B. N., . . . Souders, L. (2012). Striatal amyloid plaque density predicts Braak neurofibrillary stage and clinicopathological Alzheimer's disease: implications for amyloid imaging. *J Alzheimers Dis, 28*(4), 869-876. doi:10.3233/JAD-2011-111340

Blanken, A. E., Hurtz, S., Zarow, C., Biado, K., Honarpisheh, H., Somme, J., . . . Apostolova, L. G. (2017). Associations between hippocampal morphometry and neuropathologic markers of Alzheimer's disease using 7 T MRI. *Neuroimage Clin, 15*, 56-61. doi:10.1016/j.nicl.2017.04.020

Boyle, P. A., Yu, L., Wilson, R. S., Leurgans, S. E., Schneider, J. A., & Bennett, D. A. (2018). Person-specific contribution of neuropathologies to cognitive loss in old age. *Ann Neurol, 83*(1), 74-83. doi:10.1002/ana.25123

Braak, H., & Braak, E. (1991). Alzheimer's disease affects limbic nuclei of the thalamus. *Acta Neuropathol, 81*(3), 261-268.

Braak, H., & Braak, E. (1997). Frequency of stages of Alzheimer-related lesions in different age categories. *Neurobiol Aging, 18*(4), 351-357.

Cabinio, M., Saresella, M., Piancone, F., LaRosa, F., Marventano, I., Guerini, F. R., . . . Clerici, M. (2018). Association between Hippocampal Shape, Neuroinflammation, and Cognitive Decline in Alzheimer's Disease. *J Alzheimers Dis, 66*(3), 1131-1144. doi:10.3233/JAD-180250

Carmichael, O., Xie, J., Fletcher, E., Singh, B., DeCarli, C., & Alzheimer's Disease Neuroimaging, I. (2012). Localized hippocampus measures are associated with Alzheimer pathology and cognition independent of total hippocampal volume. *Neurobiol Aging, 33*(6), 1124 e1131-1141. doi:10.1016/j.neurobiolaging.2011.08.016

Carson, N., Leach, L., & Murphy, K. J. (2018). A re-examination of Montreal Cognitive Assessment (MoCA) cutoff scores. *Int J Geriatr Psychiatry, 33*(2), 379-388. doi:10.1002/gps.4756

Chetelat, G. (2013). Alzheimer disease: Abeta-independent processes-rethinking preclinical AD. *Nat Rev Neurol, 9*(3), 123-124. doi:10.1038/nrneurol.2013.21

Chetelat, G., Villemagne, V. L., Pike, K. E., Baron, J. C., Bourgeat, P., Jones, G., . . . Lifestyle Study of Ageing Research, G. (2010). Larger temporal volume in elderly with high versus low beta-amyloid deposition. *Brain, 133*(11), 3349-3358. doi:10.1093/brain/awq187

Cho, S. H., Shin, J. H., Jang, H., Park, S., Kim, H. J., Kim, S. E., . . . Alzheimer's Disease Neuroimaging, I. (2018). Amyloid involvement in subcortical regions predicts cognitive decline. *Eur J Nucl Med Mol Imaging*. doi:10.1007/s00259-018-4081-5

Csernansky, J. G., Wang, L., Joshi, S., Miller, J. P., Gado, M., Kido, D., . . . Miller, M. I. (2000). Early DAT is distinguished from aging by high-dimensional mapping of the hippocampus. Dementia of the Alzheimer type. *Neurology, 55*(11), 1636-1643.

Csernansky, J. G., Wang, L., Swank, J., Miller, J. P., Gado, M., McKeel, D., . . . Morris, J. C. (2005). Preclinical detection of Alzheimer's disease: hippocampal shape and volume predict dementia onset in the elderly. *Neuroimage, 25*(3), 783-792. doi:10.1016/j.neuroimage.2004.12.036

de Flores, R., La Joie, R., & Chetelat, G. (2015). Structural imaging of hippocampal subfields in healthy aging and Alzheimer's disease. *Neuroscience, 309*, 29-50. doi:10.1016/j.neuroscience.2015.08.033

Edmonds, E. C., Bangen, K. J., Delano-Wood, L., Nation, D. A., Furst, A. J., Salmon, D. P., . . . Alzheimer's Disease Neuroimaging, I. (2016). Patterns of Cortical and Subcortical Amyloid Burden across Stages of Preclinical Alzheimer's Disease. *J Int Neuropsychol Soc, 22*(10), 978-990. doi:10.1017/S1355617716000928

Fan, Z., Brooks, D. J., Okello, A., & Edison, P. (2017). An early and late peak in microglial activation in Alzheimer's disease trajectory. *Brain, 140*(3), 792-803. doi:10.1093/brain/aww349

Fischl, B., Salat, D. H., Busa, E., Albert, M., Dieterich, M., Haselgrove, C., . . . Dale, A. M. (2002). Whole brain segmentation: automated labeling of neuroanatomical structures in the human brain. *Neuron, 33*(3), 341-355.

Fischl, B., van der Kouwe, A., Destrieux, C., Halgren, E., Segonne, F., Salat, D. H., . . . Dale, A. M. (2004). Automatically parcellating the human cerebral cortex. *Cereb Cortex, 14*(1), 11-22.

Grothe, M. J., Barthel, H., Sepulcre, J., Dyrba, M., Sabri, O., Teipel, S. J., & Alzheimer's Disease Neuroimaging, I. (2017). In vivo staging of regional amyloid deposition. *Neurology, 89*(20), 2031-2038. doi:10.1212/WNL.0000000000004643

Hamelin, L., Lagarde, J., Dorothee, G., Leroy, C., Labit, M., Comley, R. A., . . . Clinical, I. t. (2016). Early and protective microglial activation in Alzheimer's disease: a prospective study using 18F-DPA-714 PET imaging. *Brain, 139*(Pt 4), 1252-1264. doi:10.1093/brain/aww017

Hanseeuw, B. J., Betensky, R. A., Mormino, E. C., Schultz, A. P., Sepulcre, J., Becker, J. A., . . . Harvard Aging Brain, S. (2018a). PET staging of amyloidosis using striatum. *Alzheimers Dement*. doi:10.1016/j.jalz.2018.04.011

Hanseeuw, B. J., Jonas, V., Jackson, J., Betensky, R. A., Rentz, D. M., Johnson, K. A., . . . Donovan, N. J. (2018b). Association of anxiety with subcortical amyloidosis in cognitively normal older adults. *Mol Psychiatry*. doi:10.1038/s41380-018-0214-2

Heneka, M. T., Carson, M. J., El Khoury, J., Landreth, G. E., Brosseron, F., Feinstein, D. L., . . . Kummer, M. P. (2015). Neuroinflammation in Alzheimer's disease. *Lancet Neurol, 14*(4), 388-405. doi:10.1016/S1474-4422(15)70016-5

Hsu, P. J., Shou, H., Benzinger, T., Marcus, D., Durbin, T., Morris, J. C., & Sheline, Y. I. (2015). Amyloid burden in cognitively normal elderly is associated with preferential hippocampal subfield volume loss. *J Alzheimers Dis, 45*(1), 27-33. doi:10.3233/JAD-141743

Iglesias, J. E., Augustinack, J. C., Nguyen, K., Player, C. M., Player, A., Wright, M., . . . Alzheimer's Disease Neuroimaging, I. (2015). A computational atlas of the hippocampal formation using ex vivo, ultra-high resolution MRI: Application to adaptive segmentation of in vivo MRI. *Neuroimage, 115*, 117-137. doi:10.1016/j.neuroimage.2015.04.042

Jack, C. R., Jr., Knopman, D. S., Jagust, W. J., Shaw, L. M., Aisen, P. S., Weiner, M. W., . . . Trojanowski, J. Q. (2010). Hypothetical model of dynamic biomarkers of the Alzheimer's pathological cascade. *Lancet Neurol, 9*(1), 119-128. doi:10.1016/S1474-4422(09)70299-6

Jack, C. R., Jr., Wiste, H. J., Weigand, S. D., Therneau, T. M., Lowe, V. J., Knopman, D. S., . . . Petersen, R. C. (2017). Defining imaging biomarker cut points for brain aging and Alzheimer's disease. *Alzheimers Dement, 13*(3), 205-216. doi:10.1016/j.jalz.2016.08.005

Jenkinson, M., Beckmann, C. F., Behrens, T. E., Woolrich, M. W., & Smith, S. M. (2012). Fsl. *Neuroimage, 62*(2), 782-790. doi:10.1016/j.neuroimage.2011.09.015

Kalin, A. M., Park, M. T., Chakravarty, M. M., Lerch, J. P., Michels, L., Schroeder, C., . . . Leh, S. E. (2017). Subcortical Shape Changes, Hippocampal Atrophy and Cortical Thinning in Future Alzheimer's Disease Patients. *Front Aging Neurosci, 9*, 38. doi:10.3389/fnagi.2017.00038

Klunk, W. E., Engler, H., Nordberg, A., Wang, Y., Blomqvist, G., Holt, D. P., . . . Langstrom, B. (2004). Imaging brain amyloid in Alzheimer's disease with Pittsburgh Compound-B. *Ann Neurol, 55*(3), 306-319. doi:10.1002/ana.20009

Leh, S. E., Kalin, A. M., Schroeder, C., Park, M. T., Chakravarty, M. M., Freund, P., . . . Michels, L. (2016). Volumetric and shape analysis of the thalamus and striatum in amnestic mild cognitive impairment. *J Alzheimers Dis, 49*(1), 237-249. doi:10.3233/JAD-150080

Lindberg, O., Walterfang, M., Looi, J. C., Malykhin, N., Ostberg, P., Zandbelt, B., . . . Wahlund, L. O. (2012). Hippocampal shape analysis in Alzheimer's disease and frontotemporal lobar degeneration subtypes. *J Alzheimers Dis, 30*(2), 355-365. doi:10.3233/JAD-2012-112210

Mitchell, A. S. (2015). The mediodorsal thalamus as a higher order thalamic relay nucleus important for learning and decision-making. *Neurosci Biobehav Rev, 54*, 76-88. doi:10.1016/j.neubiorev.2015.03.001

Murray, M. E., Lowe, V. J., Graff-Radford, N. R., Liesinger, A. M., Cannon, A., Przybelski, S. A., . . . Dickson, D. W. (2015). Clinicopathologic and 11C-Pittsburgh compound B implications of Thal amyloid phase across the

Alzheimer's disease spectrum. *Brain, 138*(Pt 5), 1370-1381. doi:10.1093/brain/awv050

Nichols, T. E., & Holmes, A. P. (2002). Nonparametric permutation tests for functional neuroimaging: a primer with examples. *Hum Brain Mapp, 15*(1), 1-25.

Nikelski, J., Chertkow, H., & Evans, A. (2012). *Running with the Beagle: A Multi-Modal, Integrative Imaging Pipeline Specialized for the Processing of Elderly Brains*. Paper presented at the Human Amyloid Imaging Conference.

Parbo, P., Ismail, R., Hansen, K. V., Amidi, A., Marup, F. H., Gottrup, H., . . . Brooks, D. J. (2017). Brain inflammation accompanies amyloid in the majority of mild cognitive impairment cases due to Alzheimer's disease. *Brain, 140*(7), 2002-2011. doi:10.1093/brain/awx120

Parbo, P., Ismail, R., Sommerauer, M., Stokholm, M. G., Hansen, A. K., Hansen, K. V., . . . Brooks, D. J. (2018). Does inflammation precede tau aggregation in early Alzheimer's disease? A PET study. *Neurobiol Dis, 117*, 211-216. doi:10.1016/j.nbd.2018.06.004

Patenaude, B., Smith, S. M., Kennedy, D. N., & Jenkinson, M. (2011). A Bayesian model of shape and appearance for subcortical brain segmentation. *Neuroimage, 56*(3), 907-922. doi:10.1016/j.neuroimage.2011.02.046

Schroeder, C., Park, M. T., Germann, J., Chakravarty, M. M., Michels, L., Kollias, S., . . . Leh, S. E. (2016). Hippocampal shape alterations are associated with regional Abeta load in cognitively normal elderly individuals. *Eur J Neurosci*. doi:10.1111/ejn.13408

Seo, S. W., Ayakta, N., Grinberg, L. T., Villeneuve, S., Lehmann, M., Reed, B., . . . Rabinovici, G. D. (2017). Regional correlations between [(11)C]PIB PET and post-mortem burden of amyloid-beta pathology in a diverse neuropathological cohort. *Neuroimage Clin, 13*, 130-137. doi:10.1016/j.nicl.2016.11.008

Smith, S. M., & Nichols, T. E. (2009). Threshold-free cluster enhancement: addressing problems of smoothing, threshold dependence and localisation in cluster inference. *Neuroimage, 44*(1), 83-98. doi:10.1016/j.neuroimage.2008.03.061

Tang, X., Holland, D., Dale, A. M., Younes, L., Miller, M. I., & Alzheimer's Disease Neuroimaging, I. (2014). Shape abnormalities of subcortical and ventricular structures in mild cognitive impairment and Alzheimer's disease: detecting, quantifying, and predicting. *Hum Brain Mapp, 35*(8), 3701-3725. doi:10.1002/hbm.22431

Tanner, J. J., McFarland, N. R., & Price, C. C. (2017). Striatal and Hippocampal Atrophy in Idiopathic Parkinson's Disease Patients without Dementia: A Morphometric Analysis. *Front Neurol, 8*, 139. doi:10.3389/fneur.2017.00139

Thal, D. R., Rub, U., Orantes, M., & Braak, H. (2002). Phases of A beta-deposition in the human brain and its relevance for the development of AD. *Neurology, 58*(12), 1791-1800.

Tzourio-Mazoyer, N., Landeau, B., Papathanassiou, D., Crivello, F., Etard, O., Delcroix, N., . . . Joliot, M. (2002). Automated anatomical labeling of activations in SPM using a macroscopic anatomical parcellation of the MNI MRI single-subject brain. *Neuroimage, 15*(1), 273-289. doi:10.1006/nimg.2001.0978

Villemagne, V. L., Burnham, S., Bourgeat, P., Brown, B., Ellis, K. A., Salvado, O., . . . Lifestyle Research, G. (2013). Amyloid beta deposition, neurodegeneration, and

cognitive decline in sporadic Alzheimer's disease: a prospective cohort study. *Lancet Neurol, 12*(4), 357-367. doi:10.1016/S1474-4422(13)70044-9

Villemagne, V. L., Pike, K. E., Chetelat, G., Ellis, K. A., Mulligan, R. S., Bourgeat, P., . . . Rowe, C. C. (2011). Longitudinal assessment of Abeta and cognition in aging and Alzheimer disease. *Ann Neurol, 69*(1), 181-192. doi:10.1002/ana.22248

Villeneuve, S., Rabinovici, G. D., Cohn-Sheehy, B. I., Madison, C., Ayakta, N., Ghosh, P. M., . . . Jagust, W. (2015). Existing Pittsburgh Compound-B positron emission tomography thresholds are too high: statistical and pathological evaluation. *Brain, 138*(Pt 7), 2020-2033. doi:10.1093/brain/awv112

Winkler, A. M., Ridgway, G. R., Webster, M. A., Smith, S. M., & Nichols, T. E. (2014). Permutation inference for the general linear model. *Neuroimage, 92*, 381-397. doi:10.1016/j.neuroimage.2014.01.060

Xia, C., Makaretz, S. J., Caso, C., McGinnis, S., Gomperts, S. N., Sepulcre, J., . . . Dickerson, B. C. (2017). Association of In Vivo [18F]AV-1451 Tau PET Imaging Results With Cortical Atrophy and Symptoms in Typical and Atypical Alzheimer Disease. *JAMA Neurol, 74*(4), 427-436. doi:10.1001/jamaneurol.2016.5755

Yi, H. A., Moller, C., Dieleman, N., Bouwman, F. H., Barkhof, F., Scheltens, P., . . . Vrenken, H. (2016). Relation between subcortical grey matter atrophy and conversion from mild cognitive impairment to Alzheimer's disease. *J Neurol Neurosurg Psychiatry, 87*(4), 425-432. doi:10.1136/jnnp-2014-309105

Yu, L., Petyuk, V. A., Gaiteri, C., Mostafavi, S., Young-Pearse, T., Shah, R. C., . . . Bennett, D. A. (2018). Targeted brain proteomics uncover multiple pathways to Alzheimer's dementia. *Ann Neurol, 84*(1), 78-88. doi:10.1002/ana.25266

Zanchi, D., Giannakopoulos, P., Borgwardt, S., Rodriguez, C., & Haller, S. (2017). Hippocampal and Amygdala Gray Matter Loss in Elderly Controls with Subtle Cognitive Decline. *Front Aging Neurosci, 9*, 50. doi:10.3389/fnagi.2017.00050

TABLES

Table 1. Demographic and clinical characteristics of participants

Variable	Participants (n=103)
Demographics	
Age, years	73.4 (6.2)
Men, n (%)	26 (25%)
Education, years	13.7 (3.2)
GDS, /30	3.1 (2.6)
General cognitive measures†	
MoCA score, /30	27.3 (2.0)
WAIS-IV: Full scale IQ	104.8 (12.0)
WMS-III: Logical Memory, immediate recall, /25	14.4 (4.0)
WMS-III: Logical Memory, delayed recall, /25	17.6 (3.1)
PiB retention values	
Global SUVr	1.25 (0.17)
Cortical SUVr	1.24 (0.18)
Left hippocampus	1.43 (0.10)
Right hippocampus	1.41 (0.09)
Left amygdala	1.45 (0.12)
Right amygdala	1.34 (0.11)
Left caudate	1.25 (0.16)
Right caudate	1.28 (0.14)
Left putamen	1.53 (0.18)
Right putamen	1.55 (0.19)
Left pallidum	1.55 (0.19)
Right pallidum	1.68 (0.16)
Left thalamus	1.24 (0.12)
Right thalamus	1.23 (0.10)

Data are presented as mean (SD).

†A detailed neuropsychological assessment was performed in every participant although only global cognitive measures are reported here.

GDS = Geriatric Depression Scale; IQ = intellectual quotient; MoCA = Montreal Cognitive Assessment; PiB = Pittsburgh compound B; SUVr = standardized uptake value ratio; WAIS-IV = Wechsler Adult Intelligence Scale—Fourth Edition; WMS-III = Wechsler Memory Scale—Third Edition.

Table 2. Global subcortical volumes and hippocampal subfields volumes in cognitively normal individuals.

Hemisphere	Structure	Volume, mm^3
Global volume		
Estimated total intracranial volume		1,370,211 (143,572)
Subcortical global volumes		
Left hemisphere	Hippocampus	3,637 (450)
	Amygdala	1,422 (237)
	Putamen	4,108 (489)
	Caudate nucleus	3,061 (373)
	Pallidum	1,816 (254)
	Thalamus	5,953 (691)
Right hemisphere	Hippocampus	3,738 (453)
	Amygdala	1,478 (222)
	Putamen	4,155 (517)
	Caudate nucleus	3,141 (373)
	Pallidum	1,725 (251)
	Thalamus	5,984 (675)
Hippocampal subfields volumes		
Left hemisphere	Subiculum	396 (53)
	CA1	565 (82)
	Hippocampal fissure	160 (28)
	Presubiculum	290 (39)
	Parasubiculum	62 (12)
	Molecular layer	508 (70)
	GC-ML-DG	265 (41)
	CA2/3	188 (34)
	CA4	231 (35)
	Fimbria	64 (20)

	HATA	54 (10)
	Hippocampal tail	506 (70)
Right hemisphere	Subiculum	396 (50)
	CA1	590 (82)
	Hippocampal fissure	165 (29)
	Presubiculum	275 (40)
	Parasubiculum	57 (11)
	Molecular layer	519 (69)
	GC-ML-DG	273 (40)
	CA2/3	201 (33)
	CA4	238 (34)
	Fimbria	59 (19)
	HATA	56 (9)
	Hippocampal tail	532 (74)

Subcortical and hippocampal subfields volumes are presented as raw mean measurements in mm^3 (SD).

CA = cornu ammonis; GC-ML-DG = granule cell and molecular layers of the dentate gyrus; HATA = hippocampal amygdala transition area.

Table 3. Associations between Aβ accumulation in subcortical structures and subcortical surface using shape considering volume and shape only analyses in cognitively normal individuals.

Clusters associated with regional PiB retention	Hemi-sphere	Number of vertices	MNI152 coordinates			F value	*r* value	*p* value
			x	y	z			
Shape considering volume analyses								
Hippocampus	Left	999	-33	-34	-9	22.2	0.442	<0.001
Hippocampus	Right	259	24	-14	-27	10.1	0.376	<0.001
		187	33	-32	-6	10.6	0.299	0.002
Thalamus	Left	2752	-3	-13	-3	17.4	0.351	<0.001
Thalamus	Right	2225	22	-32	-4	17.0	0.331	0.001
Pallidum	Right	285	22	-1	3	11.3	0.255	0.010
		109	17	-7	-6	15.4	0.331	0.001
Shape only analyses								
Thalamus	Left	162	-4	-26	4	13.9	-0.321	0.001
		66	-5	-9	15	11.3	0.310	0.002
Thalamus	Right	576	6	-27	0	20.7	-0.389	<0.001
		199	8	-7	15	10.6	0.299	0.002
Pallidum	Right	44	17	-6	-6	14.7	0.359	<0.001

Results are corrected for multiple comparisons using threshold-free cluster enhancement and clusters were considered significant if below a statistical threshold of $p<0.05$ using TFCE. Only clusters comprising at least 30 vertices are reported.

MNI = Montreal Neurological Institute; PiB = Pittsburgh compound B; TFCE = threshold-free cluster enhancement.

Table 4. Comparisons on demographic, cognitive, and morphological variables between groups based on our staging scheme of brain amyloidosis.

Variables	Stage 0 (n=71)	Stage 1 (n=26)	Stage 2 (n=6)	Difference? †	Post-hoc‡
Age, years	72.2 (5.5)	74.8 (6.4)	81.2 (6.6)	**p<0.001**	2<0 (p=0.001) 2<1 (p=0.044)
Sex (M/F)	17/54	6/20	3/3	p=0.340§	
Education, years	13.6 (3.2)	14.3 (3.6)	11.5 (1.5)	p=0.167	
Estimated TIV	1,366,239.8 (156,849.8)	1,378,901.5 (112,639.4)	1,379,550.2 (109,188.9)	p=0.918	
Global SUVr	1.16 (0.04)	1.38 (0.18)	1.67 (0.13)	**p<0.001**	2>1 (p<0.001) 2>0 (p<0.001) 1>0 (p<0.001)
Cortical SUVr	1.15 (0.04)	1.38 (0.19)	1.67 (0.14)	**p<0.001**	2>1 (p<0.001) 2>0 (p<0.001) 1>0 (p<0.001)
Cognition					
MoCA score	27.4 (1.9)	26.9 (2.1)	28.3 (1.5)	p=0.219	
Episodic memory, z score	0.18 (0.88)	-0.11 (1.05)	-1.42 (1.01)	**p<0.001**	2<0 (p<0.001) 2<1 (p=0.007)
Working memory, z score	0.22 (0.94)	-0.52 (0.97)	-0.38 (1.08)	**p=0.003**	1<0 (p=0.003)
Processing speed, z score	0.14 (0.95)	-0.29 (1.11)	-0.57 (0.76)	p=0.061	
Executive functions, z score	0.10 (0.85)	-0.18 (1.26)	-0.54 (1.02)	p=0.188	
Language, z score	0.10 (0.96)	-0.24 (1.08)	-0.28 (1.08)	p=0.263	
Attention, z score	0.18 (0.76)	-0.24 (1.08)	-0.94 (1.00)	**p=0.003**	2<0 (p=0.008)
Visuospatial abilities, z score	0.12 (1.02)	-0.30 (1.03)	-0.18 (0.39)	p=0.171	
Normalized volume of subcortical structures (%)					
Amygdala, left	0.104 (0.016)	0.104 (0.014)	0.100 (0.010)	p=0.807	
Amygdala, right	0.108 (0.014)	0.110 (0.010)	0.098 (0.013)	p=0.119	
Thalamus, left	0.436 (0.031)	0.437 (0.033)	0.419 (0.037)	p=0.435	

Thalamus, right	0.440 (0.031)	0.436 (0.038)	0.417 (0.041)	p=0.273	
Putamen, left	0.304 (0.031)	0.301 (0.051)	0.279 (0.022)	p=0.295	
Putamen, right	0.306 (0.031)	0.307 (0.060)	0.283 (0.018)	p=0.393	
Caudate, left	0.224 (0.025)	0.227 (0.031)	0.214 (0.028)	p=0.571	
Caudate, right	0.231 (0.025)	0.230 (0.030)	0.224 (0.032)	p=0.832	
Pallidum, left	0.133 (0.016)	0.135 (0.019)	0.122 (0.005)	p=0.199	
Pallidum, right	0.126 (0.016)	0.128 (0.017)	0.119 (0.009)	p=0.484	
Normalized hippocampal volumes (%)					
Whole hippocampus, left	0.2309 (0.0240)	0.2264 (0.0260)	0.2181 (0.0121)	p=0.377	
Whole hippocampus, right	0.2365 (0.0245)	0.2328 (0.0247)	0.2099 (0.0273)	**p=0.044**	2<0 (p=0.035)
Hippocampal tail, left	0.0377 (0.0052)	0.0362 (0.0053)	0.0342 (0.0035)	p=0.155	
Hippocampal tail, right	0.0396 (0.0052)	0.0385 (0.0053)	0.0352 (0.0042)	p=0.126	
Subiculum, left	0.0291 (0.0032)	0.0287 (0.0034)	0.0283 (0.0015)	p=0.711	
Subiculum, right	0.0293 (0.0033)	0.0291 (0.0032)	0.0253 (0.0041)	**p=0.020**	2<0 (p=0.014) 2<1 (p=0.034)
CA1, left	0.0415 (0.0048)	0.0414 (0.0061)	0.0404 (0.0042)	p=0.879	
CA1, right	0.0435 (0.0051)	0.0429 (0.0051)	0.0399 (0.0060)	p=0.239	
Hippocampal fissure, left	0.0116 (0.0020)	0.0119 (0.0014)	0.0117 (0.0021)	p=0.855	
Hippocampal fissure, right	0.0122 (0.0022)	0.0118 (0.0018)	0.0120 (0.0020)	p=0.721	
Presubiculum, left	0.0215 (0.0025)	0.0210 (0.0033)	0.0193 (0.0018)	p=0.130	
Presubiculum, right	0.0203 (0.0028)	0.0202 (0.0028)	0.0171 (0.0018)	**p=0.024**	2<0 (p=0.018) 2<1 (p=0.036)
Parasubiculum, left	0.0045 (0.0008)	0.0045 (0.0009)	0.0044 (0.0006)	p=0.872	
Parasubiculum, right	0.0042 (0.0008)	0.0042 (0.0008)	0.0041 (0.0006)	p=0.957	
Molecular layer, left	0.0375 (0.0042)	0.0367 (0.0048)	0.0357 (0.0030)	p=0.469	
Molecular layer, right	0.0384 (0.0044)	0.0379 (0.0044)	0.0341 (0.0056)	p=0.075	
GC-ML-DG, left	0.0195 (0.0025)	0.0192 (0.0028)	0.0183 (0.0019)	p=0.496	
GC-ML-DG, right	0.0201 (0.0024)	0.0198 (0.0026)	0.0183 (0.0031)	p=0.215	
CA2/3, left	0.0138 (0.0021)	0.0136 (0.0023)	0.0137 (0.0015)	p=0.920	
CA2/3, right	0.0149 (0.0020)	0.0146 (0.0020)	0.0133 (0.0023)	p=0.196	

CA4, left	0.0170 (0.0021)	0.0167 (0.0023)	0.0161 (0.0012)	p=0.557	
CA4, right	0.0175 (0.0020)	0.0173 (0.0022)	0.0161 (0.0025)	p=0.295	
Fimbria, left	0.0048 (0.0013)	0.0046 (0.0015)	0.0041 (0.0009)	p=0.485	
Fimbria, right	0.0044 (0.0011)	0.0043 (0.0014)	0.0030 (0.0015)	**p=0.022**	2<0 (p=0.016) 2<1 (p=0.048)
HATA, left	0.0039 (0.0007)	0.0040 (0.0006)	0.0037 (0.0005)	p=0.658	
HATA, right	0.0042 (0.0006)	0.0041 (0.0006)	0.0035 (0.0008)	p=0.071	

Data are presented as mean (SD). Values in bold represent differences that were significant. Note that investigation of group differences were not corrected for multiplicity and therefore remains exploratory.

†Analysis of variance.

‡Tukey's post-hoc tests.

§Fisher-Freeman-Halton exact test for contingency.

CA = cornu ammonis; GC-ML-DG = granule cell and molecular layers of the dentate gyrus; HATA = hippocampal-amygdala transition area; MoCA = Montreal Cognitive Assessment; SUVr = standardized uptake value ratio; TIV = total intracranial volume.

FIGURE LEGENDS

Figure 1. Scatterplots of the statistical trends between subcortical regional PiB retention values and normalized subcortical overall volumes and hippocampal subfields volumes in cognitively normal individuals.

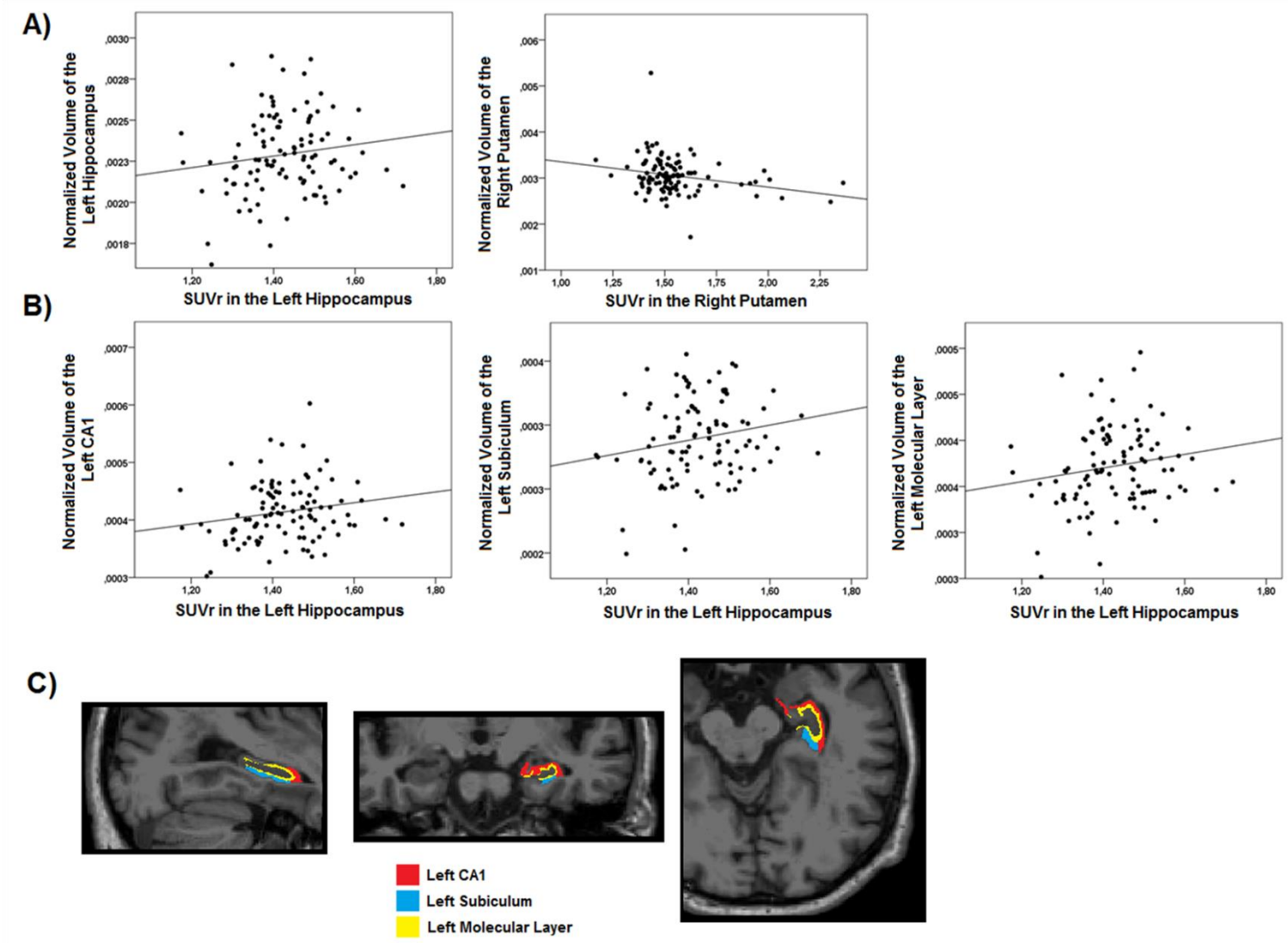

Correlations uncorrected for multiple comparisons were found between subcortical regional PiB retention values and normalized subcortical overall volumes, namely a positive relationship with the left hippocampus and a negative relationship with the right putamen (**A**). Correlations uncorrected for multiple comparisons were also found with normalized hippocampal subfields volumes, namely with the left CA1 subfield, subiculum, and molecular layer (**B**). An example of segmentation of the CA1 subfield, the subiculum, and the molecular layer from one individual from our cohort is also presented (**C**).

CA = cornu ammonis; PiB = Pittsburgh Compound B; SUVr = standardized uptake value ratio**.**

Figure 2. Associations between subcortical regional PiB retention values and subcortical surface changes due to local volume or shape in cognitively normal individuals.

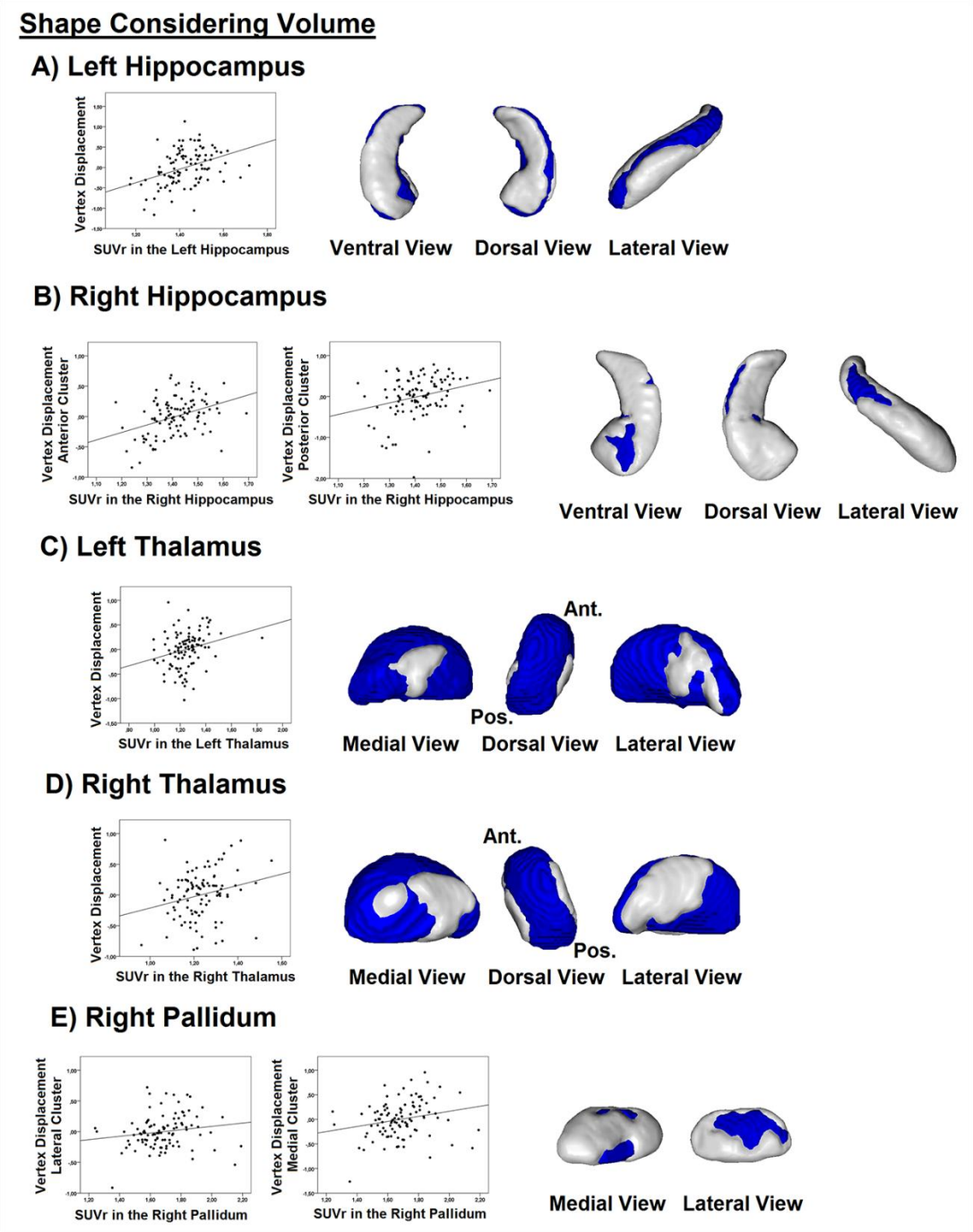

Subcortical regional PiB retention values correlated significantly with outward surface displacement when performing analyses in which surface changes are due to local volume

or shape. Positive associations were found in the bilateral hippocampus (**A, B**), the bilateral thalamus (**C, D**), and the right pallidum (**E**). No associations with surface were found in the remaining subcortical structures.

PiB = Pittsburgh Compound B; SUVr = standardized uptake value ratio.

Figure 3. Associations between subcortical regional PiB retention values and subcortical surface using analyses of shape only in cognitively normal individuals.

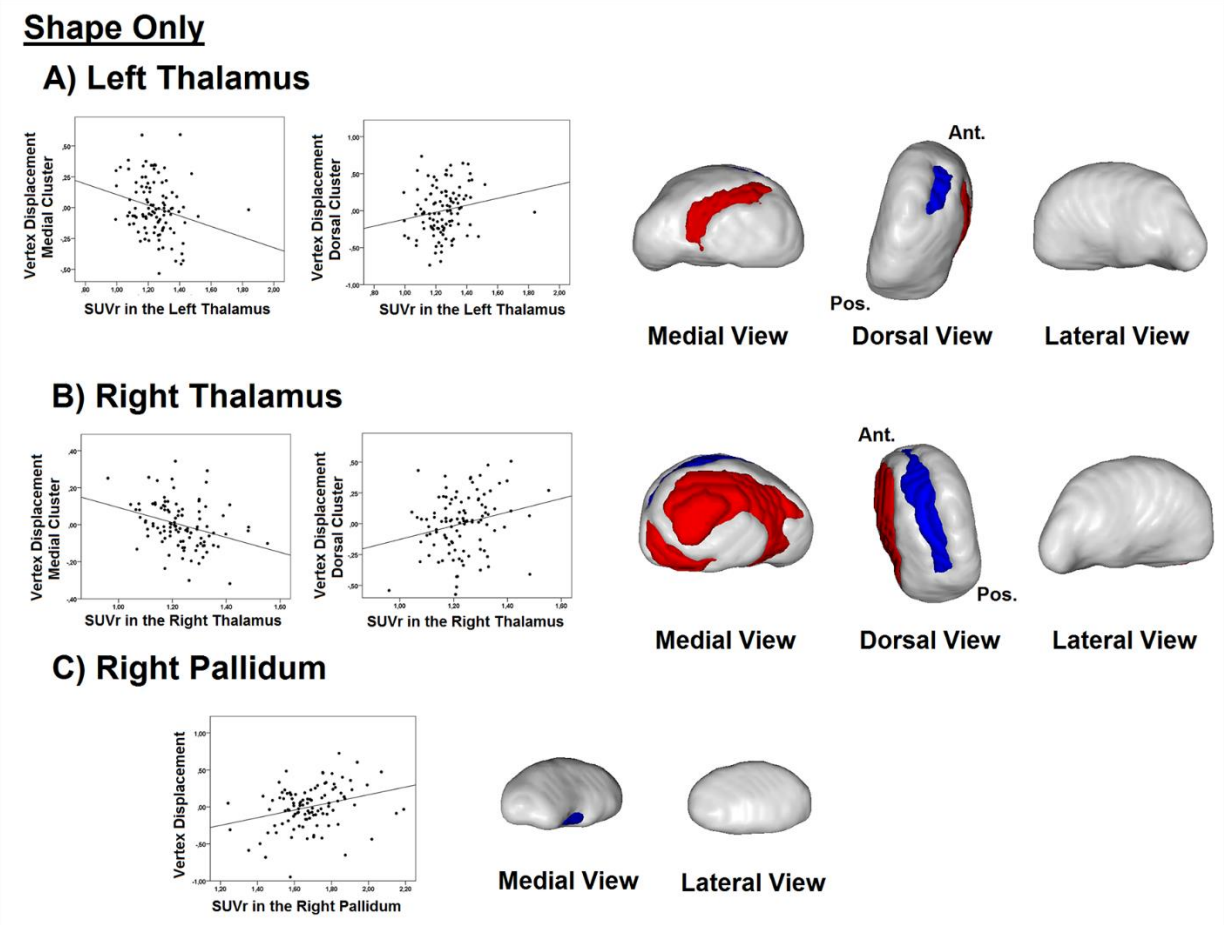

Subcortical regional PiB retention values correlated significantly with surface displacement when performing analyses in which surface changes are due to local shape only (and not local volume). Aβ-associated surface displacement was found in the bilateral thalamus (**A, B**), with inward displacement on the medial surface and outward displacement on the dorsal surface, and in the right pallidum **(C)**, with outward displacement on the ventromedial surface. Clusters in red represent negative relationships (shape contraction as regional PiB increases) and clusters in blue represent positive relationships (shape expansion as regional PiB increases).

PiB = Pittsburgh Compound B**;** SUVr = standardized uptake value ratio.

Supporting Information

SUBCORTICAL AMYLOID LOAD IS ASSOCIATED WITH SHAPE AND VOLUME IN COGNITIVELY NORMAL INDIVIDUALS

Shady Rahayel,[a,b] Christian Bocti,[c] Pénélope Sévigny Dupont,[a,b] Maude Joannette,[a,b] Marie Maxime Lavallée,[a,b] Jim Nikelski,[d] Howard Chertkow,[d,e] Sven Joubert[a,b]

Supporting Figure 1. Scatterplots of the statistical trends between subcortical regional PiB retention values and normalized subcortical overall volumes and hippocampal subfields volumes in cognitively normal individuals **when using subcortical white matter as the reference.**

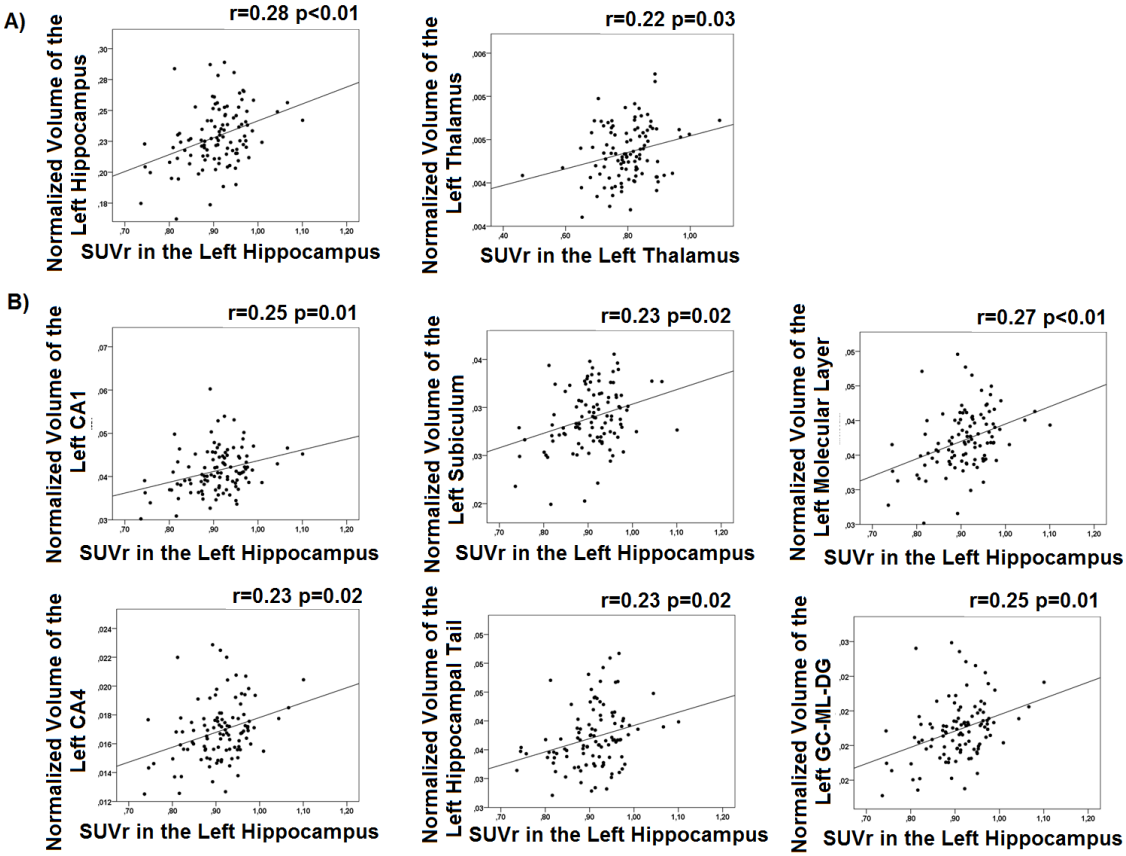

Correlations uncorrected for multiple comparisons were found between subcortical regional PiB retention values and normalized subcortical overall volumes **when using subcortical white matter as the reference**. This included a positive relationship with the left hippocampus and thalamus (**A**). Correlations uncorrected for multiple comparisons were also found with normalized hippocampal subfields volumes, namely with the left CA1 subfield, subiculum, molecular layer, CA4 subfield, hippocampal tail, and the granule cell and molecular layers of the dentate gyrus (**B**).

CA = cornu ammonis; GC-ML-DG = granule cell and molecular layers of the dentate gyrus; PiB = Pittsburgh Compound B; SUVr = standardized uptake value ratio.

Supporting Figure 2. Associations between subcortical regional PiB retention values and subcortical surface changes due to local volume or shape in cognitively normal individuals **when using subcortical white matter as the reference**.

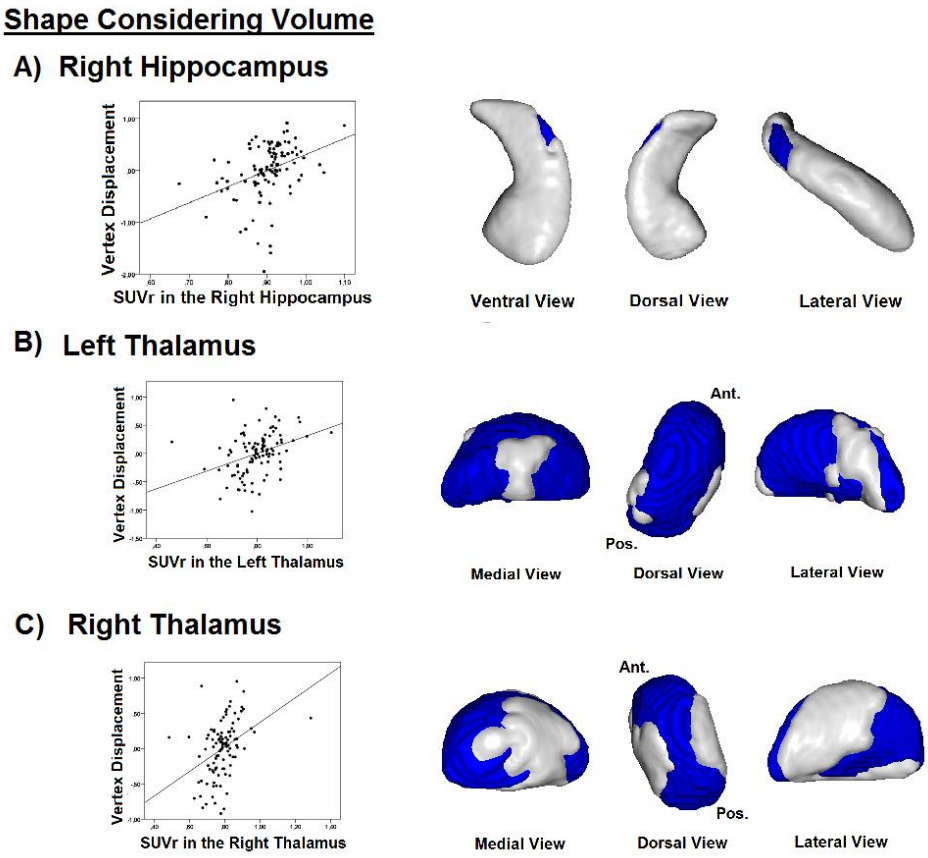

Subcortical regional PiB retention values correlated significantly with outward surface displacement when performing analyses in which surface changes are due to local volume or shape **when using subcortical white matter as the reference**. Positive associations were found in the right hippocampus (**A**) and the bilateral thalamus (**B, C**). No associations with surface were found in the remaining subcortical structures.

PiB = Pittsburgh Compound B; SUVr = standardized uptake value ratio.

Supporting Figure 3. Associations between subcortical regional PiB retention values and subcortical surface using analyses of shape only in cognitively normal individuals **when using subcortical white matter as the reference**.

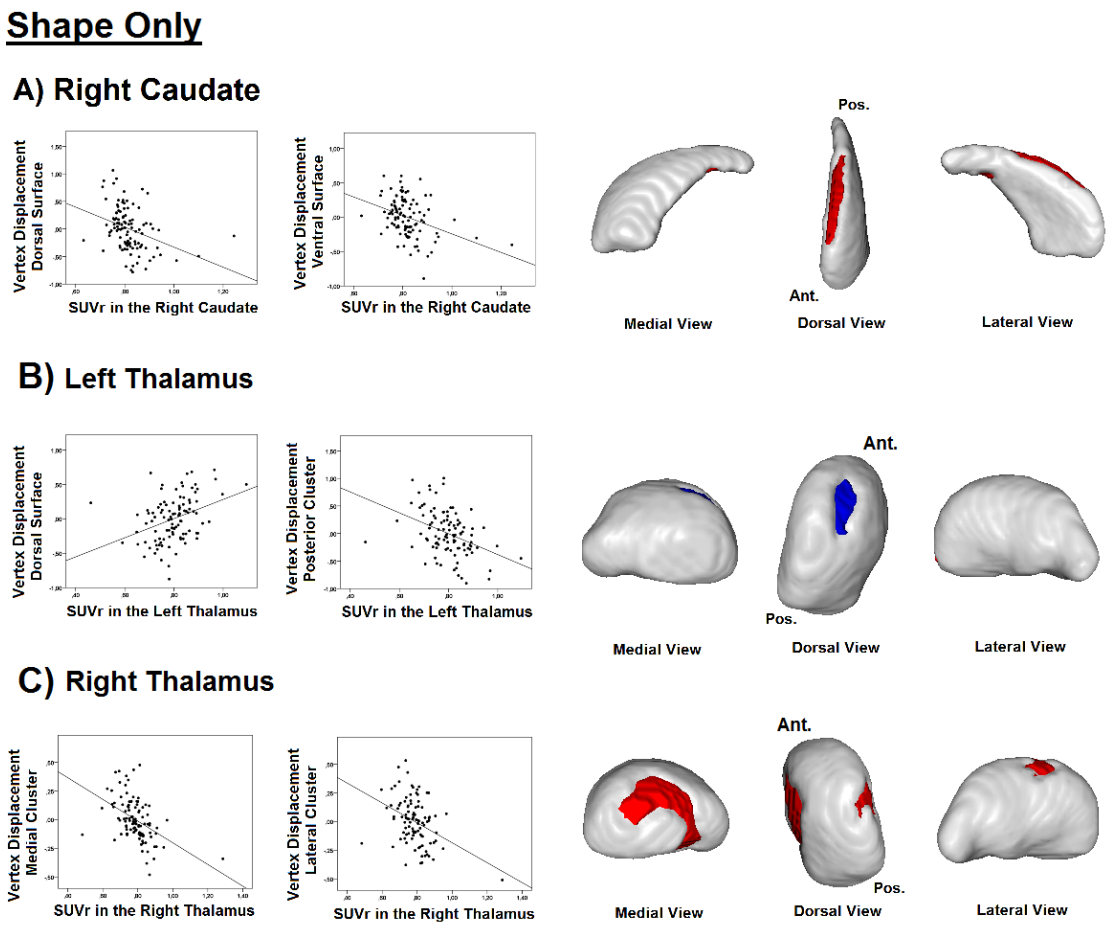

Subcortical regional PiB retention values correlated significantly with surface displacement when performing analyses in which surface changes are due to local shape only (and not local volume) **when using subcortical white matter as the reference**. Associations were found between subcortical Aβ and inward surface displacement in the right caudate (**A**), outward displacement in the left thalamus **(B)**, and inward displacement in the right thalamus **(C)**. Clusters in red represent negative relationships (shape contraction as regional PiB increases) and clusters in blue represent positive relationships (shape expansion as regional PiB increases).

PiB = Pittsburgh Compound B; SUVr = standardized uptake value ratio.

Supporting Table 1. Correlation matrix of the correlations between global, cortical, and subcortical SUVr values and subcortical overall volumes and hippocampal subfields volumes.

Structure	Global SUVr	Cortical SUVr	Hippocampal SUVr		Amygdala SUVr		Thalamus SUVr		Putamen SUVr		Caudate SUVr		Pallidum SUVr	
			Left	Right	Left	Right	Left	Right	Left	Right	Left	Right	Left	Right
Normalized volume of subcortical structures (%)														
Amygdala, left	-0.013 p=0.898	-0.016 p=0.874	-	-	-0.065 p=0.518	0.005 p=0.957	-	-	-	-	-	-	-	-
Amygdala, right	-0.058 p=0.561	-0.057 p=0.569	-	-	-0.182 p=0.069	-0.019 p=0.853	-	-	-	-	-	-	-	-
Thalamus, left	-0.053 p=0.595	-0.055 p=0.582	-	-	-	-	0.134 p=0.182	0.128 p=0.206	-	-	-	-	-	-
Thalamus, right	-0.031 p=0.758	-0.034 p=0.733	-	-	-	-	0.147 p=0.143	0.129 p=0.201	-	-	-	-	-	-
Putamen, left	-0.119 p=0.236	-0.127 p=0.207	-	-	-	-	-	-	-0.123 p=0.223	-0.184 p=0.067	-	-	-	-
Putamen, right	-0.083 p=0.410	-0.090 p=0.372	-	-	-	-	-	-	-0.122 p=0.225	**-0.214 p=0.032**	-	-	-	-
Caudate, left	-0.074 p=0.462	-0.076 p=0.448	-	-	-	-	-	-	-	-	0.127 p=0.210	0.023 p=0.823	-	-
Caudate, right	-0.078 p=0.440	-0.080 p=0.429	-	-	-	-	-	-	-	-	0.114 p=0.257	-0.019 p=0.853	-	-
Pallidum, left	-0.070 p=0.485	-0.077 p=0.444	-	-	-	-	-	-	-	-	-	-	0.067 p=0.510	0.100 p=0.321
Pallidum, right	-0.072 p=0.472	-0.078 p=0.437	-	-	-	-	-	-	-	-	-	-	0.050 p=0.620	0.124 p=0.220
Normalized hippocampal volumes (%)														
Whole hippocampus, left	-0.057 p=0.569	-0.062 p=0.537	**0.205 p=0.040**	0.065 p=0.519	-	-	-	-	-	-	-	-	-	-

Whole hippocampus, right	-0.057 p=0.573	-0.055 p=0.584	0.015 p=0.883	-0.009 p=0.930	-	-	-	-	-	-	-	-	-	-
Hippocampal tail, left	-0.086 p=0.393	-0.088 p=0.384	0.053 p=0.600	-0.040 p=0.695	-	-	-	-	-	-	-	-	-	-
Hippocampal tail, right	-0.061 p=0.546	-0.059 p=0.558	-0.069 p=0.493	-0.102 p=0.311	-	-	-	-	-	-	-	-	-	-
Subiculum, left	-0.056 p=0.577	-0.062 p=0.539	**0.248 p=0.013**	0.140 p=0.165	-	-	-	-	-	-	-	-	-	-
Subiculum, right	-0.031 p=0.759	-0.030 p=0.762	0.078 p=0.439	0.072 p=0.475	-	-	-	-	-	-	-	-	-	-
CA1, left	0.00004 p=0.9996	-0.005 p=0.960	**0.218 p=0.029**	0.082 p=0.416	-	-	-	-	-	-	-	-	-	-
CA1, right	-0.034 p=0.732	-0.033 p=0.746	0.004 p=0.971	-0.015 p=0.884	-	-	-	-	-	-	-	-	-	-
Hippocampal fissure, left	-0.022 p=0.825	-0.024 p=0.813	0.131 p=0.195	0.055 p=0.588	-	-	-	-	-	-	-	-	-	-
Hippocampal fissure, right	-0.083 p=0.410	-0.084 p=0.404	-0.001 p=0.991	-0.025 p=0.808	-	-	-	-	-	-	-	-	-	-
Presubiculum, left	-0.117 p=0.245	-0.119 p=0.234	0.148 p=0.140	0.087 p=0.388	-	-	-	-	-	-	-	-	-	-
Presubiculum, right	-0.062 p=0.541	-0.059 p=0.557	0.029 p=0.776	0.058 p=0.565	-	-	-	-	-	-	-	-	-	-
Parasubiculum, left	-0.092 p=0.360	-0.097 p=0.333	0.034 p=0.735	-0.006 p=0.950	-	-	-	-	-	-	-	-	-	-
Parasubiculum, right	-0.035 p=0.730	-0.035 p=0.725	0.099 p=0.328	0.001 p=0.994	-	-	-	-	-	-	-	-	-	-
Molecular layer, left	-0.036 p=0.718	-0.042 p=0.679	**0.241 p=0.016**	0.096 p=0.341	-	-	-	-	-	-	-	-	-	-
Molecular layer, right	-0.038 p=0.705	-0.037 p=0.717	0.025 p=0.805	0.012 p=0.903	-	-	-	-	-	-	-	-	-	-

GC-ML-DG, left	-0.036 p=0.722	-0.039 p=0.698	0.164 p=0.104	0.050 p=0.621	-	-	-	-	-	-	-	-	-	-
GC-ML-DG, right	-0.013 p=0.894	-0.013 p=0.898	0.020 p=0.840	-0.002 p=0.980	-	-	-	-	-	-	-	-	-	-
CA3, left	0.027 p=0.792	0.025 p=0.804	0.100 p=0.322	-0.025 p=0.802	-	-	-	-	-	-	-	-	-	-
CA3, right	-0.088 p=0.380	-0.086 p=0.391	-0.043 p=0.674	-0.118 p=0.244	-	-	-	-	-	-	-	-	-	-
CA4, left	-0.020 p=0.843	-0.023 p=819	0.144 p=0.153	0.014 p=0.889	-	-	-	-	-	-	-	-	-	-
CA4, right	-0.016 p=0.872	-0.016 p=0.870	0.019 p=0.849	-0.032 p=0.753	-	-	-	-	-	-	-	-	-	-
Fimbria, left	-0.087 p=0.385	-0.092 p=0.362	0.154 p=0.125	0.071 p=0.480	-	-	-	-	-	-	-	-	-	-
Fimbria, right	-0.085 p=0.397	-0.084 p=0.402	0.098 p=0.330	0.170 p=0.090	-	-	-	-	-	-	-	-	-	-
HATA, left	0.016 p=0.875	0.012 p=0.902	0.099 p=0.325	0.057 p=0.571	-	-	-	-	-	-	-	-	-	-
HATA, right	-0.049 p=0.630	-0.050 p=0.616	0.049 p=0.630	0.055 p=0.587	-	-	-	-	-	-	-	-	-	-

Cells represent the coefficient correlation with the associated significance p value. Cells indicating values in bold represent significant correlations.

CA = cornu ammonis; GC-ML-DG = granule cell and molecular layers of the dentate gyrus; HATA = hippocampal amygdala transition area; MoCA = Montreal Cognitive Assessment; SUVr = standardized uptake value ratio.